Bioorganic & Medicinal Chemistry Letters xxx (xxxx) xxxx

Contents lists available at ScienceDirect

Bioorganic & Medicinal Chemistry Letters

journal homepage: www.elsevier.com/locate/bmcl

Radiosynthesis and biological evaluation of an fluorine-18 labeled galactose derivative [^{18}F]FPGal for imaging the hepatic asialoglycoprotein receptor

Penghui Sun[a,*], Yun Zhu[b], Yanjiang Han[a], Kongzhen Hu[a], Shun Huang[a], Meng Wang[a], Hubing Wu[a], Ganghua Tang[a]

[a] Nanfang PET Center, Nanfang Hospital, Southern Medical University, Guangzhou, Guangdong Province, China
[b] Liver Tumor Center, Department of Infectious Diseases and Hepatology Unit, Nanfang Hospital, Southern Medical University, Guangzhou, Guangdong Province, China

ARTICLE INFO

Keywords:
[^{18}F]FPGal
ASGPR
Liver function imaging agent
PET imaging
Click chemistry

ABSTRACT

The asialoglycoprotein receptor (ASGPR) is abundantly expressed on the surface of hepatocytes where it recognizes and endocytoses glycoproteins with galactosyl and *N*-acetylgalactosamine groups. Given its hepatic distribution, the asialoglycoprotein receptor can be targeted by positron imaging agents to study liver function using PET imaging. In this study, the positron imaging agent [^{18}F]FPGal was designed to specifically target hepatic asialoglycoprotein receptor and its effectiveness was assessed in *in vitro* and *in vivo* models. The radiosynthesis of [^{18}F]FPGal required 50 min with total radiochemical yields of [^{18}F]FPGal from [^{18}F]fluoride as 10% (corrected radiochemical yield). The K_d of [^{18}F]FPGal to ASGPR in HepG2 cells was 1.99 ± 0.05 mM. Uptake values of 0.55% were observed within 30 min of incubation with HepG2 cells, which could be blocked by 200 mM D(+)-galactose (< 0.1%). *In vivo* biodistribution analysis showed that the liver accumulation of [^{18}F]FPGal at 30 min was 4.47 ± 0.96% ID/g in normal mice compared to 1.33 ± 0.07% ID/g in hepatic fibrotic mice ($P < 0.01$). Reduced uptake in the hepatic fibrosis mouse models was confirmed through PET/CT images at 30 min. Compared to normal mice, the standard uptake value (SUV) in the hepatic fibrosis mice was significantly lower when assessed through dynamic data collection for 1 h. Therefore, [^{18}F]FPGal is a feasible PET probe that provide insight into ASGPR related liver disease.

Hepatitis, cirrhosis and liver cancer are common liver diseases in China.[1] Liver fibrosis is an injury repair response that proceeds chronic liver injury. Chronic liver disease eventually develops into cirrhosis, the complications of which are life threatening.[2] Liver fibrosis leads to hepatic portal hypertension, hepatic ascites, synthetic dysfunction, and impaired metabolic capacity. In-depth studies of liver fibrosis have important clinical significance in relieving liver fibrosis. To-date, the clinical methods for the assessment of liver function include serum biochemical indicators, the Child-Pugh scoring system, a model for end-stage liver disease (MELD) scoring system, indocyanine green (ICG) excretion tests, and imaging examinations, such as single photon emission computed tomography (SPECT) and positron emission tomography (PET).[3–5] Whilst effective, these tests only reflect preoperative liver function, whilst the function of the resected or residual liver is not assessed prior to surgery.[6] Recently, the development of 3D-imaging techniques such as SPECT and PET/CT make it possible to evaluate the function of preoperative liver segments.[7–9]

The asialoglycoprotein receptor (ASGPR) is a liver lectin that was discovered by Ashwell and Morell during the assessment of mammalian plasma glycoprotein metabolism.[10] ASGPR is a transmembrane protein present on the surface of hepatocytes that contains 100,000–500,000 binding sites per cell. Its two major receptor subtypes include ASGPR1 and ASGPR2. ASGPR1 specifically recognizes and binds to glycoproteins with galactosyl and *N*-acetylgalactosamine groups leading to their metabolism.[11] ASGPR1 has utility as a drug target, with anticancer and antiviral drugs that bind to ASGPR1 being specifically endocytosed into liver cells, enhancing their liver targeting. Natural ligands of ASGPR include galactose, lactose, *N*-acetylgalactosamine, asialofetuin and asialo-serum mucin.[12]

Over the past four decades, several studies have reported the development of radiolabeled ASGPR ligands,[13–20] but only a few have been successfully imaged by PET or SPECT.[13,15,19] [^{99m}Tc]-NGA was the first imaging agent used to evaluate liver function.[13] In 1983, it was employed as a single photon imaging agent to acquire human SPECT images.[14] To simplify the labeling stages, Kubota and colleagues covalently linked three to four DTPA molecules to the backbone of NGA

* Corresponding author at: Nanfang PET Center, Nanfang Hospital, Southern Medical University, 1838 Guangzhou Avenue North, Guangzhou, Guangdong Province 510515, China.
E-mail address: sunsam2014@163.com (P. Sun).

https://doi.org/10.1016/j.bmcl.2020.127187
Received 25 February 2020; Received in revised form 9 April 2020; Accepted 9 April 2020
0960-894X/

albumin to obtain diethylenetriamine pentaacetate galactosyl human serum albumin (GSA) and used [^{99m}Tc] for radiochemical labeling to obtain [^{99m}Tc]-GSA,[15] which was the first commercially available receptor-binding radio- pharmaceutical. The current clinical use rates of [^{99m}Tc]-GSA in Japan are high.[9] In 2009, Yang and colleagues labeled NGA with [^{18}F]fluoride through *N*-succinimidyl-4-^{18}F-fluoro-benzoate ([^{18}F]SFB) to obtain a novel PET tracer [^{18}F]FNGA.[16] The PET tracer [^{18}F]FNGA showed favorable biological properties highlighting its potential application for the assessment of hepatocyte function with PET/CT. However, the relatively low radiochemical yields proved an obstacle to its clinical application. In 2010, Yang et al. labeled galactosyl chitosan with ^{18}F through [^{18}F]SFB to obtain a novel PET tracer [^{18}F]FB-GC.[17] Despite its promising biological properties, [^{18}F]FB-GC was limited for clinical applications due to its complex labeling process and low final radiolabeling yield. In 2013, Kao et al. reported a novel PET probe [^{18}F]FBHGal.[18] The biological characterization of [^{18}F]FBHGal suggested that it was a feasible tracer for PET imaging in hepatic fibrosis mouse models which may provide new insight into ASGPR-related liver dysfunction. In the same year, Haubner et al. reported a more clinically feasible ^{68}Ga labeled probe, [^{68}Ga]GSA.[19] The ease of preparation based on commercial GSA kits provided a promising prospective for [^{68}Ga]GSA during liver function imaging with PET. Recently, Gupta et al. reported three IDA radiopharmaceuticals for clinical use.[20] These included [^{99m}Tc]lidofenin (HIDA), [^{99m}Tc]disofenin (DISIDA) and [^{99m}Tc]mebrofenin (BrIDA). Of these agents, [^{99m}Tc]Mebrofenin displayed the highest levels of hepatic extraction, blood clearance and lowest renal excretion. Whilst these studies have improved liver function assays,[13,15,16,18,19] ^{18}F-labeled monoantagonal galactoside shows promise for more accurate liver assessments.

In this study, we designed and radiosynthesized a fluorine-18 labeled galactose derivative 4-(2-[^{18}F]fluoropropyl)-1-β-D-galactopyranosyl-1,2,3-triazole ([^{18}F]FPGal). We used the "click reaction" to label 1-deoxy-β-D-galactopyranosyl azide with 5-[^{18}F]fluoro-1-pentyne. The 1,2,3-triazole scaffold was featured in a vast number of bioactive molecules which have exhibited considerable biological and pharmaceutical activities.[21–23] [^{19}F]FPGal was synthesized in four steps from β-D-galactose pentaacetate (Scheme 1). The synthetic process was relatively complex and the cold reference compound [^{19}F]FPGal had a purity ≥ 90% and a yield ≥ 34% (See Supporting information for all product data including ^{1}H NMR, ^{19}F NMR and mass spectrometry).

The radiosynthesis of [^{18}F]FPGal was initiated with fluorine-18 and 5-(p-toluenesulfonyl)-1-yne to obtain 5-[^{18}F]fluoro-1-pentyne in a PET-MF-2V-IT-I synthesizer module (Scheme 2). This product was then reacted with 1-deoxy-β-D-galactopyranosyl azide using "click chemistry" to obtain the final product. The radiosynthesis yield of [^{18}F]FNGA was 8–10% and the total reaction time was 150 min. Compared to [^{18}F]FNGA, the radiosynthesis yields of [^{18}F]FPGal were comparable, but the overall synthesis times were over 3-three times longer than those of [^{18}F]FPGal. Therefore, the advantage of [^{18}F]FPGal is that comparable yields can be obtained in a shorter synthesis time.

The [^{18}F]FPGal was a colorless and clear solution of pH 7.0 and a radiochemical purity of ≥ 99%. Typical [^{18}F]FPGal spectra were determined through analytical radioactivity HPLC (Fig. 1). The retention time of the cold reference [^{19}F]FPGal was 11.05 min (Fig. 1A) and the [^{18}F]FPGal's retention time was 11.15 min (Fig. 1B), indicating that [^{18}F]FPGal was the target product. The radiochemical purity was ≥ 99% and the specific activity of [^{18}F]FPGal was 6.85 MBq/μmol.

The octanol–water partition coefficient for [^{18}F]FPGal was determined through the assessment of its distribution in *n*-octanol and water (pH = 7.4). The lipophilicity logP value of [^{18}F]FPGal at pH 7.4 was −1.45 ± 0.07 (n = 3), indicating that the compound was hydrophilic.

The cellular uptake of [^{18}F]FPGal was evaluated in hepatocellular carcinoma (HCC) HepG2 cells (Fig. 2A). HepG2 cells express high levels of ASGPR and the uptake of [^{18}F]FPGal was rapid and moderately high, reaching 0.55% within 30 min of incubation. Incubation with 200 mM of D(+)-galactose blocked HepG2 cellular uptake (< 0.1%), indicating that the binding of [^{18}F]FPGal was ASGPR-specific. The K_d of [^{18}F]FPGal was assessed at different concentrations of [^{18}F]FPGal (6.85 MBq/μmol) to HepG2 cells in 24-well plates. The K_d value of [^{18}F]FPGal to ASGPR in HepG2 cells was 1.99 ± 0.05 mM (Fig. 2B), which was much lower than the K_d of ^{131}I-YEEE(α-ah-GalNAc)$_3$ (K_d = 0.1 μM). By comparing the K_d values of [^{18}F]FPGal and ^{131}I-YEEE (α-ah-GalNAc)$_3$, we can know that the binding affinity of [^{18}F]FPGal was very low, thus leading to its low uptake in HepG2 cells.

Twelve Kunming 4-week old mice weighing 20 g were purchased from the Animal Experimental Center of Southern Medical University (Guangzhou China). Animal models of liver fibrosis were produced using 20% carbon tetrachloride induction.[24] Briefly, carbon tetrachloride/peanut oil at a volume ratio of 20% was administered to the abdominal cavity at a dose of 2 mL/kg twice a week for 6 weeks. Mice were sacrificed and liver function was assessed through pathological HE staining and blood biochemical indicators. The results of pathological HE staining are shown in Fig. 3C and D.

The results of serum biochemical indicators showed that alanine aminotransferase (ALT) values were 12-fold higher in the model group compared to the control group, and the aspartate aminotransferase (AST) detection values in the model group were 7-fold higher than the control group (Fig. 3B). In most cases, the elevated levels of ALT and AST were consistent with the degree of hepatocyte damage. Further assessments of body weight, liver morphology, HE staining and blood serum biochemical indicators indicated the successful production of the liver fibrosis model.

[^{18}F]FPGal displayed good stability in PBS for up to 2 h, as analyzed by a reserve-phase HPLC. The result showed that the percentage of intact probe remains > 95% after 2 h incubation at 37 °C (Fig. 4B). [^{18}F]FPGal also has good stability in liver at 1 h (Fig. 4C). Metabolite analysis revealed that [^{18}F]FPGal was slowly metabolized *in vivo*, with 30% of intact probe in plasma at 1 h after injection, and defluorination was not observed (Fig. 4D).

Biodistribution of [^{18}F]FPGal was assessed in Kunming mice at 5 and 30 min to evaluate the distribution pattern of the radiofluorinated compound *in vivo*. Table 1 shows the data obtained expressed as the percentage of the total injected dose per gram of tissue (% ID/g). At 30 min, the liver uptake was 4.47 ± 0.97 %ID/g in normal mice, while that in the hepatic fibrosis mice was significantly reduced

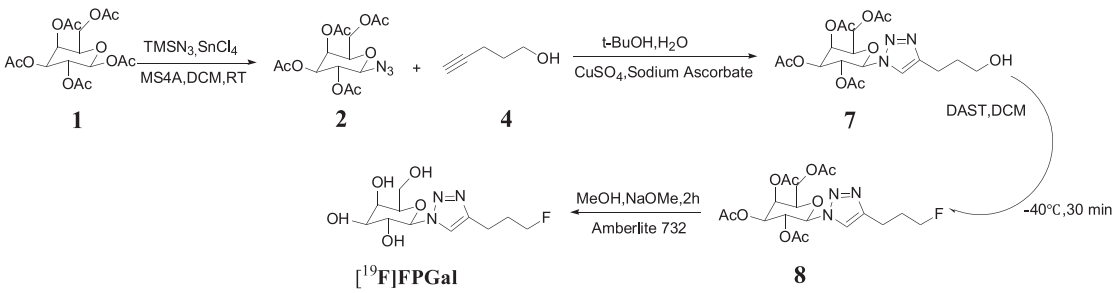

Scheme 1. Synthesis of [^{19}F]FPGal.

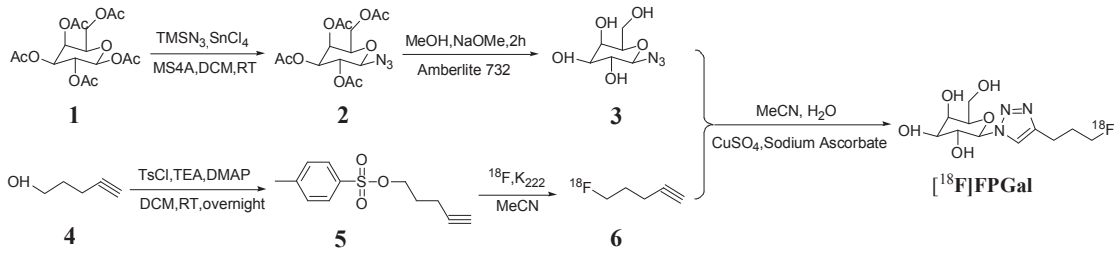

Scheme 2. Synthesis of [^{18}F]FPGal.

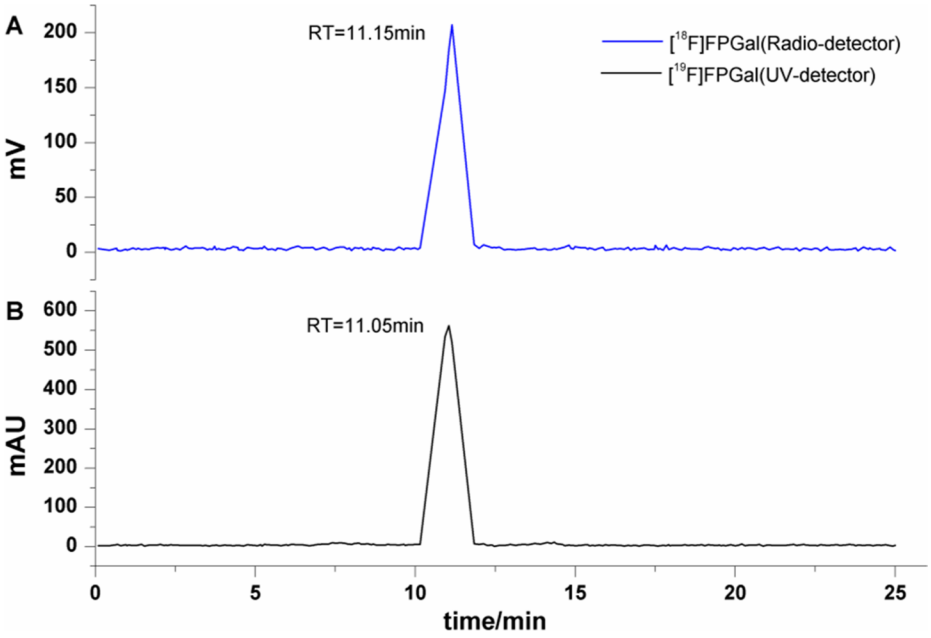

Fig. 1. Analytical HPLC of [^{18}F]FPGal (RT = 11.15 min) (A) and standard references of [^{19}F]FPGal (RT = 11.05 min) (B). RT = retention time.

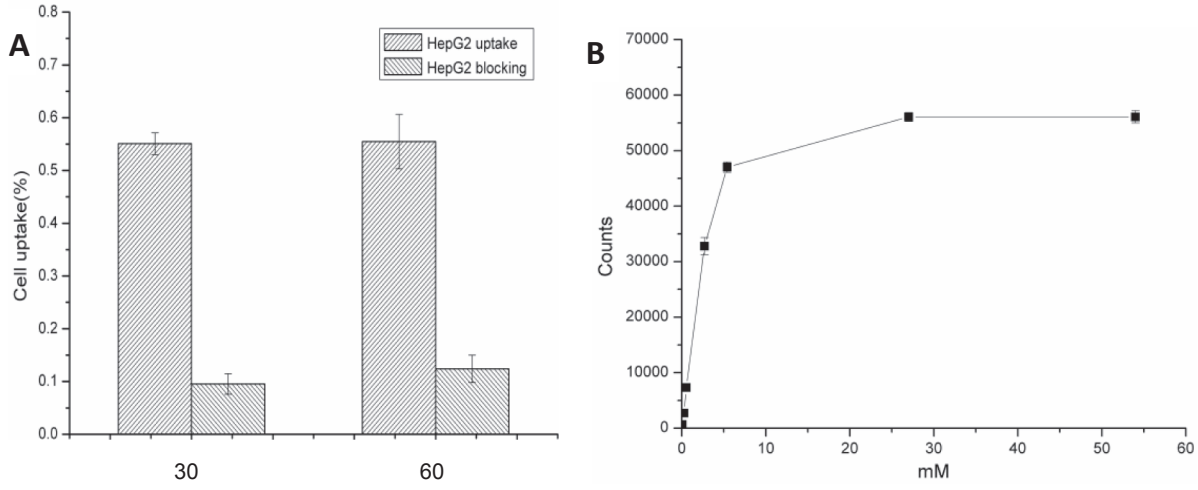

Fig. 2. Cell uptake studies of [^{18}F]FPGal in 30 and 60 min using HepG2 tumor cells (ASGP receptor-positive) (n = 3). Blocking studies in 30 and 60 min with 200 mM D(+)-galactose confirmed the receptor-specific uptake (A). Binding saturation curve of [^{18}F]FPGal to ASGPR in HepG2 cell lines (B). Values are represented as means ± SD, n = 3.

(1.33 ± 0.07 %ID/g, P < 0.01). Besides, the L/M ratio in normal mice and in hepatic fibrisis mice at 30 min was 22.35 and 4.59, respectively. The differences in liver uptakes between normal and hepatic fibrosis mice, though not remarkable in [^{18}F]FPGal PET imaging, still reached statistical significance in biodistribution study (P < 0.01). Besides, rapid blood clearance of [^{18}F]FPGal in the hepatic fibrosis mice was noticed, which leads to a close liver/blood ratio in model group and control group (1.95 *vs* 1.96, P > 0.01). The reason may be that lower binding affinity and faster *in vivo* metabolism result in a lower liver/ background ratio, which is bad for a good probe. The kidney uptake in control group increased from 10.33 ± 1.99 %ID/g (5 min) to 15.68 ± 4.3 %ID/g (30 min), while that in model group decreased

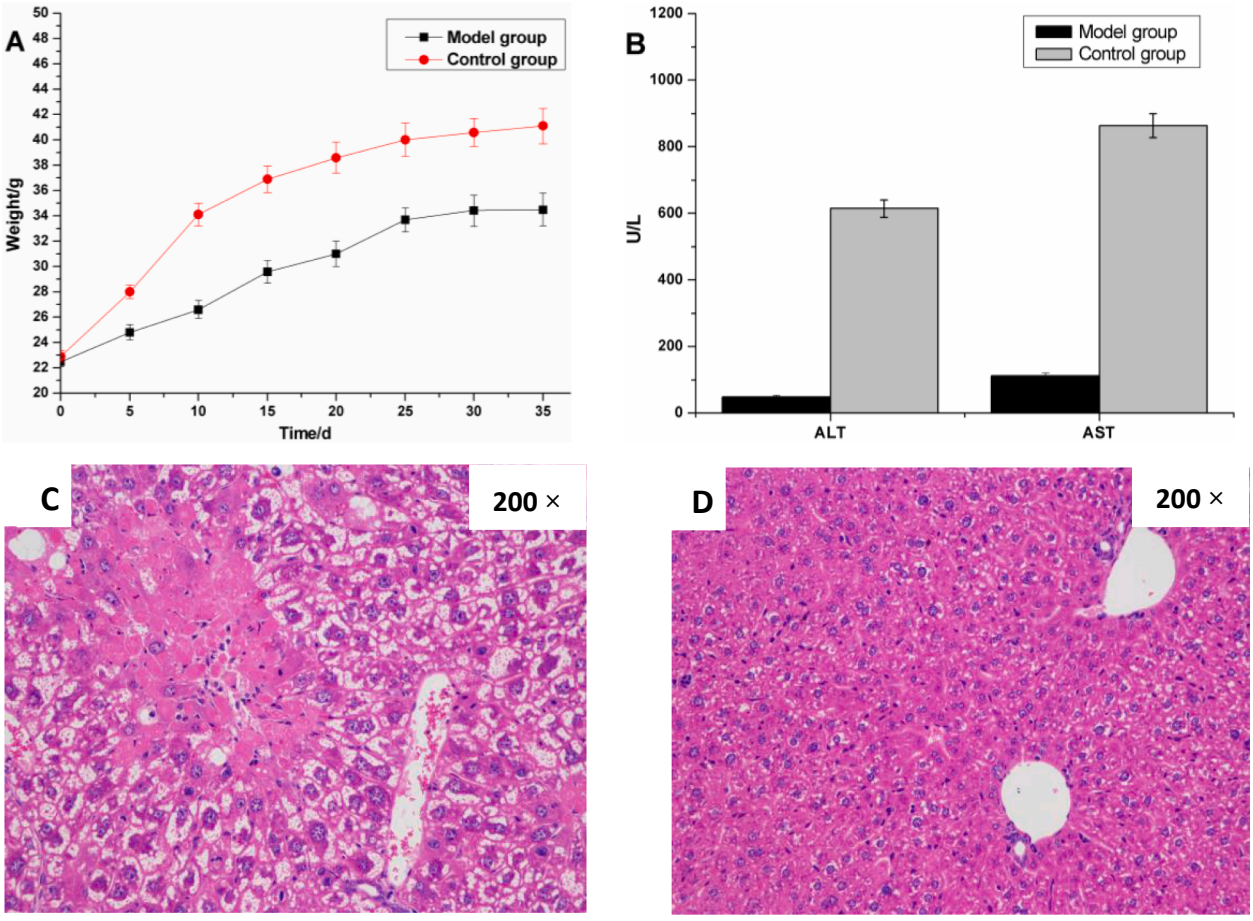

Fig. 3. Body weight changes in model and control groups (A). Comparison of serum ALT and AST (B). HE staining in the model (200×) (C) and control groups (200×) (D). Values are represented as means ± SD, n = 3.

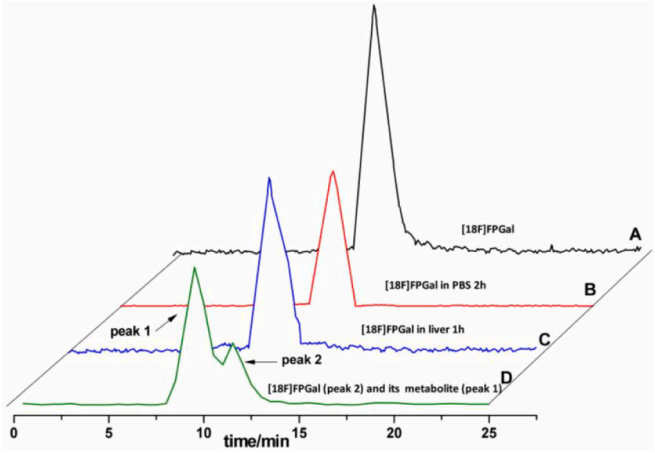

Fig. 4. Radioactive HPLC analysis of [^{18}F]FPGal (A), [^{18}F]FPGal in PBS at 2 h (B), [^{18}F]FPGal in liver at 1 h (C) and the metabolite (peak 1) of [^{18}F]FPGal at 1 h (D).

from 13.13 ± 1.24 %ID/g (5 min) to 3.92 ± 1.67 %ID/g (30 min). Moreover, higher radioactivity levels in the kidney indicated that [^{18}F]FPGal were primarily excreted through the kidneys. In addition, the levels of [^{18}F]FPGal uptake in other organs of interest (bone, muscle, brain and gallbladder) were relatively low. Moreover, the biodistribution of [^{18}F]FPGal is similar to that of [^{18}F]FB-GC.[17] At 30 min, the radioactivity mainly accumulated in the urinary bladder and kidney, followed by the liver, while the radioactive uptakes of other organs were not high. Besides, the liver uptake value of [^{18}F]FPGal in normal mice was 4.47 ± 0.97% ID/g, while the uptake value of [^{18}F]FB-GC in normal mice was > 10% ID/g ($P < 0.01$), the reason for the difference may be that [^{18}F]FPGal is a strong hydrophilic tracer, which leads to its relatively rapid metabolism in the body. Furthermore, it also may be that the binding affinity of [^{18}F]FPGal for ASGPR is not as high as that of [^{18}F]FB-GC.

Dynamic micro PET/CT studies were performed with [^{18}F]FPGal. PET images at 5 and 30 min are shown in Fig. 5A-B, and blocking PET images of hepatic fibrosis mice at 30 and 60 min are shown in Fig. 5C. From the PET images at 30 min (Fig. 5A-B), the liver uptake of hepatic fibrosis mice were visually lower than normal mice. High kidney and bladder uptake were observed in both groups. Rapid kidney uptake was visualized in the first 1520 min of the model group. Maximum kidney uptake was achieved within the first 20 min after injection, then slowly decreased throughout the 60 min scan time. While in the control group, maximum kidney uptake was reached within the first 30 min post-injection, then slowly decreased throughout the 60 min scan time, suggesting that the metabolism of the kidneys was affected when liver function was reduced. The speed of absorption of the tracer was also affected.

In this study, we used a semi-quantitative indicator standard uptake value (SUV) to compare the liver of the model group and the control group. At 5 min, the mean SUVs of liver in model group and control group were 0.81 ± 0.14 and 0.90 ± 0.15, respectively, $P < 0.01$. While at 30 min, the mean SUVs of liver in model group and control group were 0.80 ± 0.10 and 0.98 ± 0.11, respectively, $P < 0.01$ (Fig. 5D). The SUV results of liver in both groups had significant statistical difference, which can be considered as a useful diagnostic

Table 1
Biodistribution in model and control groups at 5 min and 30 min after the intravenous injection of [^{18}F]FPGal. Values are represented as means ± SD, n = 3.

	Control group		Model group	
	5 min	30 min	5 min	30 min
Bone	0.74 ± 0.21	0.75 ± 0.27	0.35 ± 0.26	0.27 ± 0.06
Muscle	0.53 ± 0.22	0.20 ± 0.10	0.55 ± 0.06	0.29 ± 0.15
Lung	1.86 ± 0.76	0.76 ± 0.25	2.52 ± 0.07	0.76 ± 0.06
Brain	0.13 ± 0.05	0.17 ± 0.13	0.15 ± 0.03	0.05 ± 0.03
Heart	1.31 ± 0.93	0.60 ± 0.38	1.08 ± 0.07	0.37 ± 0.08
Liver	2.75 ± 0.70	4.47 ± 0.97	2.67 ± 0.10	1.33 ± 0.07
Kidney	10.33 ± 1.99	15.69 ± 4.30	13.13 ± 1.24	3.92 ± 1.67
Spleen	0.80 ± 0.41	2.08 ± 0.59	1.11 ± 0.04	0.86 ± 0.43
Gallbladder	0.82 ± 0.71	0.44 ± 0.18	0.74 ± 0.10	0.39 ± 0.27
Stomach	0.46 ± 0.18	0.90 ± 0.20	0.58 ± 0.31	0.3 ± 0.17
Intestine	1.72 ± 0.52	2.42 ± 0.21	2.1 ± 0.69	0.82 ± 0.06
Urinary bladder	1.36 ± 0.24	99.81 ± 21.73	7.64 ± 1.87	133.45 ± 25.06
Blood	2.10 ± 1.15	2.28 ± 0.41	2.45 ± 0.22	0.68 ± 0.13
Liver/Muscle	5.19	22.35	4.85	4.59
Liver/Heart	2.10	7.45	2.47	3.59
Liver/Blood	1.31	1.96	1.09	1.95

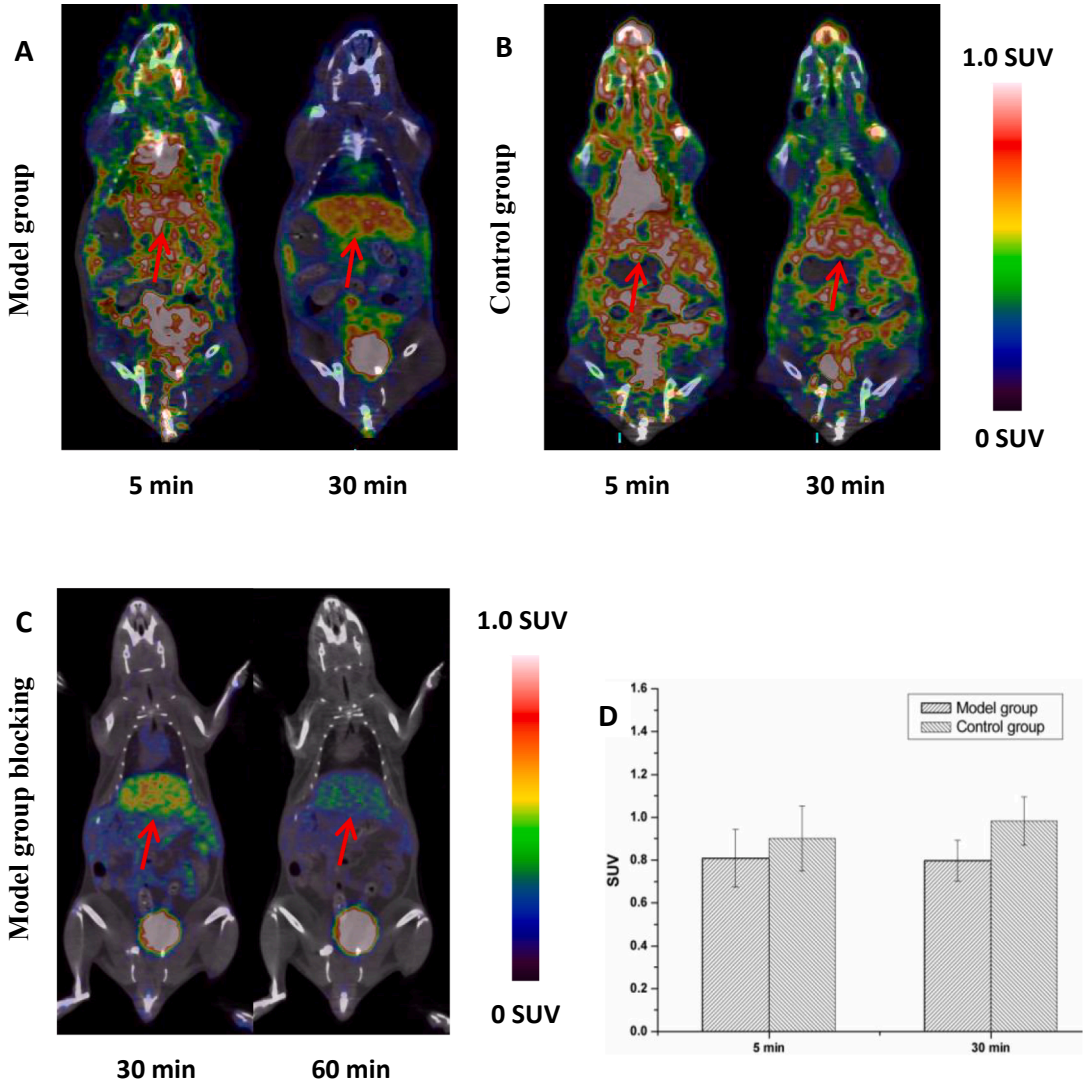

Fig. 5. Micro-PET/CT images of [^{18}F]FPGal in hepatic fibrosis mice (model group) 5, 30 min after intravenous injection (A). Micro-PET/CT images of [^{18}F]FPGal in Kunming mice (control group) at 5, 30 min intravenous injection (B). Micro PET/CT images of the blocking experiment in hepatic fibrosis mice (model group) at 30, 60 min post-intravenous injection (C). The SUV of liver derived from micro PET images (D). (n = 3 per group; bars represent means ± SD).

Table 2
The SUV of liver derived from micro PET in control group, model group and blocking group at 30 and 60 min after the intravenous injection of [^{18}F]FPGal. (n = 3 per group; values represent means ± SD.)

	Time (min)	Model group	Blocking group
SUV (liver)	30	0.80 ± 0.10	0.64 ± 0.09
	60	0.66 ± 0.11	0.42 ± 0.07

parameter in estimating the dysfunction of hepatocytes. For comparison, blocking experiments were performed using 200 mM of pre-injected D(+)-galactose (20 mg/kg of body weight) 5 min prior to the intravenous injection of the radiotracer on hepatic fibrosis mice. As shown, the liver uptake of the blocking group was visually lower than control mice. Similarly, we use the SUV to evaluate the effect of blocking (Table 2). At 30 min, the mean SUVs of liver in model group and blocking group derived from micro PET images were 0.80 ± 0.10 and 0.64 ± 0.09, respectively, $P < 0.01$. While at 60 min, the mean SUVs of liver in model group and blocking group derived from micro PET images were 0.66 ± 0.11 and 0.42 ± 0.07, respectively, $P < 0.01$. From the PET results of blocking experiment in model group we can know that the blocking was effective but not obvious. While in the PET blocking experiment of [^{18}F]FNGA, the authors used free NGA as blocking agent (10 mg/kg rats body weight), leading to low uptake in liver.[16] Therefore, we concluded that the PET imaging experiments were carried out under partially blocking conditions due to the low specific activity, resulting in a low uptake in both model group and control group. In addition, because of the relative bad blocking effect of D(+)-galactose, we need to use a better inhibitor to do the blocking experiment in the later research.

In conclusion, we have successfully radiosynthesized a novel positron imaging agent 4-(2-[^{18}F]fluoropropyl)-1-β-D-galactopyranosyl-1,2,3-triazole ([^{18}F]FPGal) as a molecular probe that specifically targets ASGPR. *In vitro* assays and *in vivo* PET/CT imaging and biodistribution studies showed that [^{18}F]FPGal exhibits relatively low affinity for the ASGP receptor. In addition, [^{18}F]FPGal showed relatively high liver accumulation and low accumulation in other organs or tissues (bone, muscle, brain), resulting in a high target/non-target ratio. Therefore, [^{18}F]FPGal is a feasible PET probe that provide insight into ASGPR related liver disease.

Declaration of Competing Interest

The authors declare that they have no known competing financial interests or personal relationships that could have appeared to influence the work reported in this paper.

Acknowledgments

This work was supported by grants from President Foundation Project of Nanfang Hospital, Southern Medical University (2015C004), Science and Technology Planning Project of Guangdong Province of China (2014A020212175), and President Foundation Project of Nanfang Hospital, Southern Medical University (2018Z003).

Appendix A. Supplementary data

Supplementary data to this article can be found online at https://doi.org/10.1016/j.bmcl.2020.127187.

References

1. Yang T, Wu MC. Discrimination against hepatitis B carriers in China. *Lancet.* 2011;378:1059.
2. Friedman SL. Molecular regulation of hepatic fibrosis, an integrated cellular response to tissue injury. *J Biol Chem.* 2000;275:2247–2250.
3. Wang YY, Zhao XH, Ma L, et al. Comparison of the ability of Child-Pugh score, MELD score, and ICG-R15 to assess preoperative hepatic functional reserve in patients with hepatocellular carcinoma. *J Surg Oncol.* 2018;118:440–445.
4. Khisti Rohit Patidar, Garg Yashwant, Mukund Lalit, et al. Correlation of baseline portal pressure (hepatic venous pressure gradient) and indocyanine green clearance test with post-transarterial chemoembolization acute hepatic failure. *J Clin Exp Hepatol.* 2019;9:447–452.
5. Horowitz JM, Venkatesh SK, Ehman RL, et al. Evaluation of hepatic fibrosis: a review from the society of abdominal radiology disease focus panel. *Abdom Radiol.* 2017;42:2037–2053.
6. van Roekel Caren, Reinders Margot TM, van der Velden Sandra, et al. Hepatobiliary imaging in liver-directed treatments. *Semin Nucl Med.* 2019;49:227–236.
7. Bateman TM. Advantages and disadvantages of PET and SPECT in a busy clinical practice. *J Nucl Cardiol.* 2012;19:3–11.
8. de Graaf W, Bennink RJ, Veteläinen R, van Gulik TM. Nuclear imaging techniques for the assessment of hepatic function in liver surgery and transplantation. *J Nucl Med.* 2010;51:742–752.
9. Kaibori M, Ha-Kawa SK, Maehara M, et al. Usefulness of Tc-99m-GSA scintigraphy for liver surgery. *Ann Nucl Med.* 2011;25:593–602.
10. Morell AG, Irvine RA, Sternlieb I, Scheinberg H. Physical and chemical studies on ceruloplasmin. V. Metabolic studies on sialic acid-free ceruloplasmin in vivo. *J Biol Chem.* 1968;243:155–159.
11. Li KB, Li N, Zang Y, et al. Foldable glycoprobes capable of fluorogenic crosslinking of biomacromolecules. *Chem Sci.* 2016;7:6325–6329.
12. Ma Y, Chen H, Su S, et al. Galactose as broad ligand for multiple tumor imaging and therapy. *J Cancer.* 2015;6:658–670.
13. Vera DR, Stadalnik RC, Krohn KA. Technetium-99m galactosyl-neoglyco-albumin: preparation and preclinical studies. *J Nucl Med.* 1985;26:1157–1167.
14. Stadalnik Robert C, Vera David R. The evolution of 99mTc-NGA as a clinically useful receptor-binding radiopharmaceutical. *Nucl Med Biol.* 2001;28:499–503.
15. Kubota Y, Kojima M, Hazama H, et al. A new liver function test using the asialoglycoprotein receptor system on the liver cell membrane: I. evaluation of liver imaging using Tc-99m-neoglycoprotein. *Jpn J Nucl Med.* 1986;23:899–905.
16. Yang W, Mou T, Peng C, et al. Fluorine-18 labeled galactosyl-neoglycoalbumin for imaging the hepatic asialoglycoprotein receptor. *Bioorg Med Chem.* 2009;17:7510–7516.
17. Yang W, Mou T, Guo W, et al. Fluorine-18 labeled galactosylated chitosan for asialoglycoprotein-receptor-mediated hepatocyte imaging. *Bioorg Med Chem Lett.* 2010;20:4840–4844.
18. Kao HW, Chen CL, Chang WY, et al. [18]F-FBHGal for asialoglycoprotein receptor imaging in a hepatic fibrosis mouse model. *Bioorg Med Chem.* 2013;21:912–921.
19. Haubner R, Vera DR, Farshchi-Heydari S, et al. Development of ^{68}Ga-labelled DTPA galactosyl human serum albumin for liver function imaging. *Eur J Nucl Med Mol Imaging.* 2013;40:1245–1255.
20. Gupta Manoj, Choudhury Partha Sarathi, Singh Shivendra, Hazarika Dibyamohan. . Liver functional volumetry by Tc-99m mebrofenin hepatobiliary scintigraphy before major liver resection: a game changer. *Indian J Nucl Med.* 2018;33:277–283.
21. Kharb R, Sharma PC, Yar MS. Pharmacological signifificance of triazole scaffold. *J Enzyme Inhib Med Chem.* 2011;26:1–21.
22. Thirumurugan P, Matosiuk D, Jozwiak K. Click chemistry for drug development anddiverse chemical-biology applications. *Chem Rev.* 2013;113:4905–4979.
23. Horne WS, Yadav MK, Stout CD, Ghadiri MR. Heterocyclic peptide backbone modifications in an alpha-helical coiled coil. *J Am Chem Soc.* 2004;126:15366–15367.
24. Sun H, Che QM, Zhao X, Pu XP. Antifibrotic effects of chronic baicalein administration in a CCl4 liver fibrosis model in rats. *Eur J Pharmacol.* 2010;631:53–60.